



On the Application of the Optical Method of Caustics to the Investigation of Transient Elastodynamic Crack Problems: Limitations of the Classical Interpretation

Ares J. Rosakis, Sridhar Krishnaswamy* & Hareesh V. Tippur

Graduate Aeronautical Laboratories, California Institute of Technology, Pasadena, California 91125, USA

ABSTRACT

Several possible sources of inaccuracy that occur in the classical interpretation of caustics patterns generated during transient crack growth in elastic materials are examined using a 'Bifocal Caustics' set-up and a new full field optical technique called 'Coherent Gradient Sensing'. During unsteady dynamic crack growth, strict K_I^d -dominance is generally absent, especially at times close to crack initiation and arrest, even in regions outside the crack-tip 3-D zone where plane stress conditions persist. In such cases a truly transient higher order expansion is found to be essential for correctly describing stress fields outside the 3-D zone.

1 INTRODUCTION

The optical method of caustics is a widely used technique in experimental solid mechanics. In the area of fracture mechanics, in particular, it has been one of the primary tools of investigation of catastrophic failure, starting with the pioneering works of Manogg,¹ and continuing over the years through the efforts of Theocaris,² Beinert & Kalthoff,³ Rosakis *et al.*,⁴ Zehnder & Rosakis,⁵ Ravi-Chandar & Knauss,⁶ among others.

The technique has several advantages over other optical methods

* Present address: Department of AMES, University of California at San Diego, La Jolla, California 92093, USA.

which are mainly related to its simplicity. It requires a simple optical experimental set-up which does not involve the use of diffraction optics. It can be used easily either in transmission or in reflection mode. Data analysis is simple and does not require the use of complicated image processing techniques. The simplicity of the technique makes it an ideal candidate for high speed photography applications. In particular, the fact that the physical principle of caustics does not hinge on the availability of a coherent, monochromatic light source has allowed for the use of high-speed camera systems, which utilize white light illumination (for example, spark gap cameras of the Crazz–Schardin type). In addition, the lack of complicated optical components, such as diffraction gratings, beam splitters, etc., in a caustics set-up ensures minimal light intensity losses which are crucial for successful high-speed photography. Indeed, in such applications, light intensity is of the essence since the exposure times involved are often very short (of the order of nanoseconds).

As currently used in fracture studies, the method of caustics is subject to two sets of simplifying assumptions, one in the analysis of the optical technique, and the other regarding the nature of the mechanical fields under study. The limitations introduced by the simplifications in the optical analysis of the method of caustics as well as an exact geometrical optics interpretation of the technique are discussed in Rosakis & Zehnder.⁷ It turns out that the simplified analysis deviates from the exact geometrical analysis in only relatively extreme regimes, and, for the most part, the simplified optical analysis is adequate. The corresponding issue regarding the assumptions made about the mechanical fields under study, however, is more troublesome. Typically, interpretation of caustics data in fracture mechanics is done under the assumption that crack-tip deformation is well described by two-dimensional, steady state, asymptotic models. To the extent that these assumptions are violated in a laboratory specimen, caustics data are prone to misinterpretation and error.

In this paper, we shall first briefly describe the method of caustics as it is currently used in elastodynamic fracture studies, with particular attention paid to the approximations involved. We will then review some of the attempts that have been made in the recent past toward quantifying the errors incurred due to crack-tip three-dimensionality and possible inadequacy of a steady state, asymptotic description of the crack-tip deformation. Finally, the results from an alternate full-field optical technique (Coherent Gradient Sensing,⁸ which is sensitive to the same deformation quantities as the method of caustics), will be presented. These latter results, in particular, will be shown to

substantiate the main contention of this paper, namely: the assumptions regarding the crack-tip mechanical fields under which interpretation of caustics data is customarily made is a potential source of large errors. In conclusion, possible ways to overcome these limitations through the use of more realistic, transient, higher-order descriptions of the mechanical fields will be suggested.

2 THE OPTICAL METHOD OF CAUSTICS

2.1 The physical principle

Consider a plate specimen of uniform thickness, in the undeformed state. Let its middle cross-section occupy the x_1, x_2 plane of an orthonormal Cartesian coordinate system. The specimen is such that it causes non-uniform changes in the optical path when light is transmitted through it, or reflected from its surface. For a specimen made of a transparent material, the change in the optical path is due to non-uniform changes in the thickness of the plate and also due to gradients in the refractive index of the material. For a specimen made of an opaque material, the change in optical path is due to non-uniform surface elevations of the plate. In experimental solid mechanics, both gradients in refractive index and non-uniform thickness changes are related to gradients in the stress state which are induced when loads are applied to the boundary of the initial undeformed plate.

Consider further a collimated beam of light traveling in the x_3 -direction, normally incident on the plate, as illustrated in Fig. 1. Under certain stress gradients, the reflected or refracted rays will form an envelope in the form of a three-dimensional surface in space. This surface, which is called the *caustic surface*, is the locus of points of maximum luminosity in the reflected or transmitted light fields.

The deflected rays are tangent to the caustic surface. If a screen is positioned parallel to the $x_3 = 0$ plane, and so that it intersects the caustic surface, then the cross-section of the surface can be observed on the screen as a bright curve (the *caustic curve*) bordering a dark region (the *shadow spot*) on the screen. Suppose that the incident ray, which is reflected from or transmitted through point $p(x_1, x_2)$ on the specimen, intersects the screen at the image point $P(X_1, X_2)$. The X_1, X_2 coordinate system is identical to the x_1, x_2 system, except that the origin of the former has been translated by a distance z_0 to the screen (z_0 can be either positive or negative). The position of the image point P will

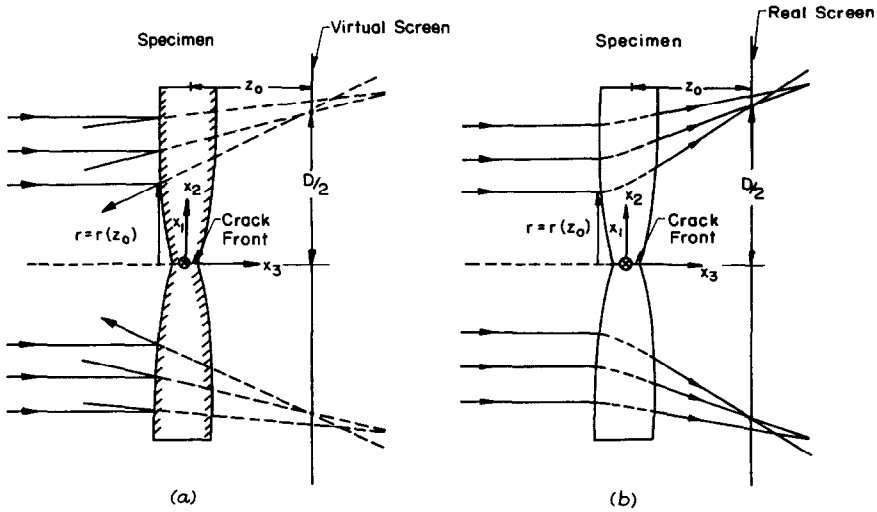


Fig. 1. Caustic formation in (a) reflection, (b) transmission.

depend on the gradient of the optical path change $\Delta S(x_1, x_2)$ introduced by the specimen as well as on the distance z_0 and is given by:⁷

$$\mathbf{X} = \mathbf{x} + z_0 \nabla(\Delta S(x_1, x_2)) \tag{1}$$

where $\mathbf{X} = X_\alpha \mathbf{e}_\alpha$, $\mathbf{x} = x_\alpha \mathbf{e}_\alpha$, and \mathbf{e}_α denote unit vectors, and '∇' denotes the two-dimensional gradient operator. In the subsequent discussions, Greek subscripts have the range 1, 2 while Latin subscripts take the values 1, 2, 3. Relation (1) describes the mapping of the points on the specimen onto points on the screen.

2.2 The initial curve and its significance

If the screen intersects the caustic surface, then the resulting caustic curve on the screen is the optical mapping of the locus of points for which the determinant of the Jacobian matrix of mapping eqn (1) must vanish on the specimen, i.e.

$$J(x_1, x_2, ; z_0) = \det [X_{\alpha,\beta}] = \det [\delta_{\alpha,\beta} + z_0(\Delta S)_{,\alpha\beta}] = 0 \tag{2}$$

Equation (2) is a necessary and sufficient condition for the existence of a caustic curve.⁷ The locus of points on the reference plane ($x_1, x_2, x_3 = 0$) for which the Jacobian vanishes is called the *initial curve* whose geometry is described by eqn (2).

For fracture mechanics applications which are relevant in this work, the plate specimen contains a stationary or running through-crack and the origin of the coordinate system is often taken to be on the crack

front at the specimen center. In such cases the initial curve is found to be a curve surrounding the crack tip, whose exact geometry and size will depend, among other things, on material constitution and on the distance of the specimen to the screen.⁷ In such cases the initial curve has some interesting properties which are briefly described below.

All points on the initial curve map onto the caustic curve. In addition, all points inside and outside this curve map outside the caustic.⁷ Since light reflected both from the inside and the outside of the initial curve maps outside the caustic, the area within the caustic remains dark and is customarily referred to as the shadow spot. An example of a caustic and shadow spot obtained by reflection of light from the vicinity of a dynamically propagating crack in AISI 4340 steel is shown in Fig. 2. The crack-tip speed in this case was approximately 1000 m/s. The circular rings surrounding the caustic and shadow spot are caustic images of stress waves generated during crack growth. Since the light that forms the caustic originates from the initial curve, essential information conveyed by the caustic comes from that curve only.

Equation (2) defining the initial curve depends parametrically on z_0 . Thus, by varying z_0 , we may vary the initial curve position. If z_0 is large, the initial curve will be far from the crack tip. If z_0 is small, the initial curve will be close to the crack tip. In a practical experimental set-up, a camera is often used to record the transmitted or reflected light fields. In this case the object plane of this camera is the 'screen' and its distance from the specimen is z_0 . In a reflection arrangement, for example, the object plane of the camera is often set behind the specimen surface and thus the image is virtual. Variation of z_0 can thus easily be achieved experimentally by simply varying the object plane of the recording camera system.

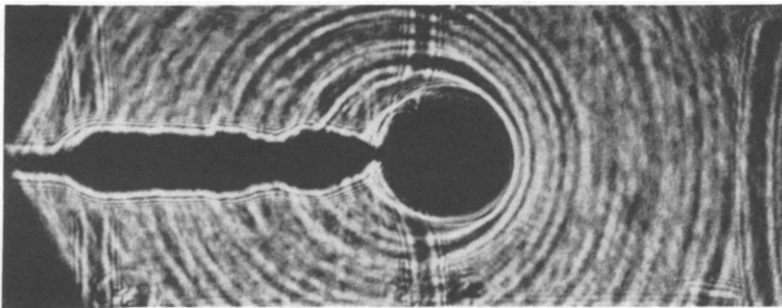


Fig. 2. Caustic of a dynamically propagating crack in an AISI 4340 steel specimen (crack speed $v \sim 1000$ m/s).

The dependence of initial curve size on z_0 is an essential property of the method of caustics, and it can be utilized to scan the near-tip region to obtain information regarding the nature of the deformation field at different distances from the crack tip. This property will be utilized extensively in the following sections.

2.3 Caustics by reflection

For opaque specimens, caustics are formed by the reflection of light rays from the polished specimen surface. The shape of the caustic curve depends on the near-tip normal displacement u_3 of the plate surface, initially at $x_3 = h/2$, where h is the undeformed specimen thickness. The change in optical path in this case is given by:

$$\Delta S(x_1, x_2) = 2u_3(x_1, x_2, h/2) = 2h \int_0^{1/2} \epsilon_{33} d(x_3/h)$$

where ϵ_{33} is the direct strain component in the thickness direction. For an isotropic, homogeneous, linear elastic solid, the above reduces to:

$$\begin{aligned} \Delta S(x_1, x_2) &= 2u_3(x_1, x_2, h/2) \\ &= \frac{-2\nu h}{E} \int_0^{1/2} \left\{ (\sigma_{11} + \sigma_{22}) \left[1 - \frac{\sigma_{33}}{\nu(\sigma_{11} + \sigma_{22})} \right] \right\} d(x_3/h) \quad (3) \end{aligned}$$

2.4 Caustics by transmission

For transparent specimens the optical path change ΔS depends on both local changes in thickness and on local changes in refractive index, and can be expressed as:

$$\Delta S(x_1, x_2) = 2h(n-1) \int_0^{1/2} \epsilon_{33} d(x_3/h) + 2h \int_0^{1/2} \Delta n d(x_3/h)$$

where n is the refractive index of the material. The first term represents the net optical path difference due to changes in plate thickness caused by the strain component ϵ_{33} . The second term is due to the stress induced change in refractive index of the material. This change in the refractive index Δn is given by the Maxwell relation,

$$\Delta n(x_1, x_2) = D_1(\sigma_{11} + \sigma_{22} + \sigma_{33})$$

where D_1 is the stress optic constant and σ_{ij} are Cartesian stress components. The above relation is strictly true for isotropic linear elastic solids. For such solids the strain component ϵ_{33} can also be related to the stresses in a straightforward manner and the change in

path length becomes:

$$\Delta S(x_1, x_2) = 2h \left(D_1 - \frac{\nu}{E} (n - 1) \right) \int_0^{1/2} \times \left\{ (\sigma_{11} + \sigma_{22}) \left[1 - D_2 \left(\frac{\sigma_{33}}{\nu(\sigma_{11} + \sigma_{22})} \right) \right] \right\} d(x_3/h) \quad (4)$$

where

$$D_2 = - \left[\frac{\nu D_1 + \frac{\nu(n-1)}{E}}{D_1 - \frac{\nu(n-1)}{E}} \right]$$

E and ν are the Young's modulus and the Poisson's ratio of the material respectively.

2.5 Interpretation of caustics on the basis of plane stress analysis

The discussion of the previous section was intentionally kept as general as possible within the assumptions of isotropic linear elasticity. For a cracked linear elastic plate of uniform thickness and finite in-plane dimensions, the optical path difference ΔS given by eqns (3) and (4) in general will depend on the details of the three-dimensional elastostatic or elastodynamic stress state that would exist at the vicinity of the crack tip. This will be a function of the applied loading, as well as of the in-plane dimensions and thickness of the specimen. Given the lack of full-field, three-dimensional analytical solutions in fracture mechanics, such information can be obtained only by means of detailed numerical calculations. Such an approach was adopted in Refs 9–11.

Nevertheless, there exist certain non-trivial special cases for which available asymptotic solutions, based on two-dimensional analyses, may provide adequate approximations for $\Delta S(x_1, x_2)$. In particular, it has been argued that conditions of generalized plane stress will dominate in thin cracked plates at distances from the crack front larger than half the specimen thickness.^{12–14} This would imply that if the initial curve is kept outside the near-tip three-dimensional zone, the resulting caustic could be interpreted on the basis of a generalized plane stress analysis.

To illustrate the extent of the near-tip three-dimensionality, reference is made to Fig. 3 which shows a 3-D representation of the ratio $(\sigma_{33}/\nu(\sigma_{11} + \sigma_{22}))$, often called the degree of plane strain. This ratio is a measure of near-tip three-dimensionality and is obtained by means of a 3-D finite element calculation, which models a stationary crack in a three-point bend specimen subjected to dynamic loading.¹⁵ In regions where the deformation is locally plane stress, this measure is equal to

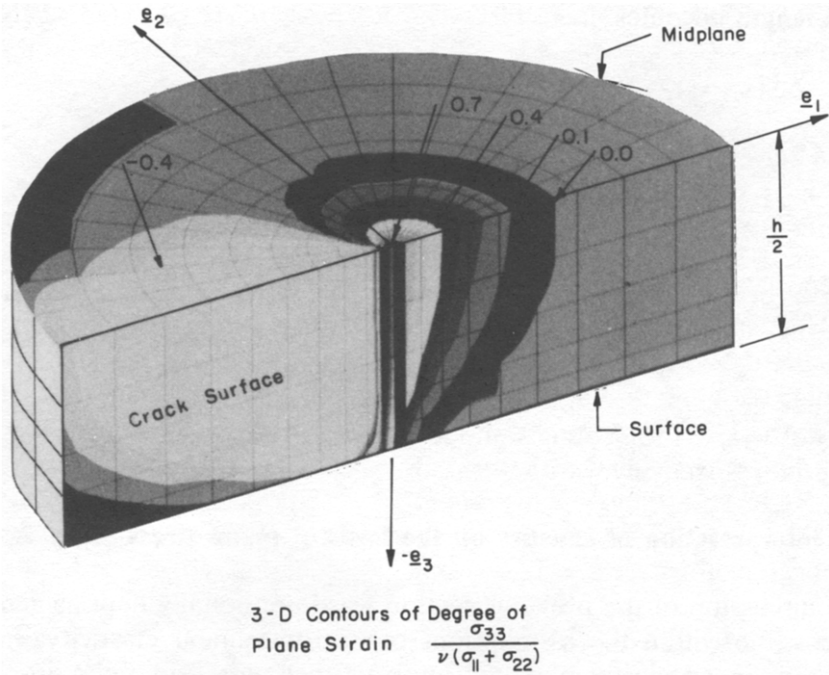


Fig. 3. Plane strain constraint near a stationary, dynamically loaded crack front in a three-point bend specimen.

zero. In the figure, only one half of the specimen thickness is shown. The top surface corresponds to the mid-plane of the specimen. The maximum extent of the 3-D zone is approximately $0.4-0.5h$. For points outside this region, a plane stress approximation will be applicable. Indeed for such points the optical path difference ΔS (eqns (3) and (4)), which involve the ratio $\sigma_{33}/\nu(\sigma_{11} + \sigma_{22})$, will simplify to:

$$\Delta S(x_1, x_2) \approx ch[\hat{\sigma}_{11}(x_1, x_2) + \hat{\sigma}_{22}(x_1, x_2)] \tag{5}$$

where

$$c = \begin{cases} \left(D_1 - \frac{\nu}{E}(n-1)\right) = c_\sigma & \text{for transmission} \\ \frac{\nu}{E} & \text{for reflection} \end{cases}$$

and $\hat{\sigma}_{11}$ and $\hat{\sigma}_{22}$ are thickness averages of the stress components in the solid. In the above expression c_σ is called the stress-optical coefficient. These stress components will be provided by the generalized plane stress solution of the elastostatic or elastodynamic problem under investigation.

3 CAUSTICS GENERATED BY DYNAMICALLY GROWING CRACKS: CLASSICAL ANALYSIS, ASSUMPTIONS AND SHORTCOMINGS

3.1 Analysis based on K_I^d -dominance

In this section we present the methodology that leads to the classical analysis of optical caustic patterns generated during dynamic crack growth in metals. We pay particular attention to the assumptions involved and we attempt to analyze some cases where these assumptions break down.

Consider a mode-I crack propagating dynamically in a thin plate composed of a homogeneous isotropic, linear elastic material. The crack-tip velocity and the dynamic stress intensity factor are both allowed to be arbitrary functions of time. If a plane stress assumption is made, then the first stress invariant $\hat{\sigma}_{11} + \hat{\sigma}_{22}$ at the vicinity of the propagating crack tip can be asymptotically expressed as:¹⁶

$$\hat{\sigma}_{11} + \hat{\sigma}_{22} = F(v) \frac{K_I^d(t)}{\sqrt{2\pi r_1}} \cos(\theta_1/2) + O(1) \quad \text{as } r_1 \rightarrow 0 \quad (6)$$

where

$$F(v) = \frac{2(1 + \alpha_s^2)(\alpha_1^2 - \alpha_s^2)}{[4\alpha_1\alpha_s - (1 + \alpha_s^2)^2]}$$

$$\alpha_{1,s} = \left(1 - \frac{v(t)^2}{c_{1,s}^2}\right)^{1/2}$$

$v(t)$ is the instantaneous crack speed, $K_I^d(t)$ is the instantaneous value of the dynamic stress intensity factor,

$$r_1 = (x_1^2 + (\alpha_1 x_2)^2)^{1/2}, \quad \theta_1 = \tan^{-1}((\alpha_1 x_2)/x_1)$$

and the distorted polar coordinate system (r_1, θ_1) translates with the moving crack tip.

From a mathematical standpoint the above expression is only the leading term of a transient asymptotic expansion for the stresses, which will be presented in Section 4. As will be seen in that section, only the leading $1/\sqrt{r_1}$ term of the transient expansion has the same form as the corresponding term of an expansion obtained if steady-state conditions are assumed. Indeed the $O(1/\sqrt{r_1})$ term of the transient problem is obtained if the constant values for K_I^d and v of the steady-state case are replaced by their time varying counterparts. However, this is not true for terms of higher order. For the transient crack growth problem, such terms will in general contain time derivatives of $v(t)$ and $K_I^d(t)$. As a result their importance relative to the leading term will depend on the

nature of the time history of crack-tip speed and stress intensity factor. In addition, the θ_1 variations of the transient higher order terms are found to be different from their steady-state counterparts of the same order in r_1 .

The classical analysis of caustics is based on the premise that in a real experimental situation, eqn (6) will approximate the stress field at least in a non-vanishing annulus defined by $b < r < a$. The inner bound b is dictated by the extent of the three-dimensional zone surrounding the crack tip (see previous section) while a is determined by the transient nature of the loading (see Section 4). A region where eqn (6) holds is called a K_I^d -dominant region.

If the optical path difference corresponding to eqns (5) and (6) is substituted in to the caustic mapping eqn (1), these become:¹⁷

$$\begin{cases} X_1 = r_1 \cos \theta_1 + \mu r_1^{-3/2} \cos \frac{3\theta_1}{2} \\ X_2 = \frac{r_1 \sin \theta_1}{\alpha_1} + \alpha_1 \mu r_1^{-3/2} \sin \frac{3\theta_1}{2} \end{cases} \quad (7)$$

where

$$\mu = \frac{z_0 hc F(v) K_I^d}{\sqrt{2\pi}}$$

If one now imposes the condition for the existence of a caustic curve, eqn (2), the equation of this curve is obtained and its maximum transverse diameter D can be related to K_I^d and v as follows:⁴

$$K_I^d(t) = G(\alpha_1) \frac{2\sqrt{2\pi} F(v(t))}{ch} [D(t)]^{5/2} \quad (8)$$

where $G(\alpha_1) = (6.8 + 14.4\alpha_1 - 2.6\alpha_1^2) \times 10^{-3}$.

For sufficiently small crack velocities ($v < 0.3c_s$) the locus of points on the specimen (the initial curve) that maps onto the caustic is very nearly circular and its nominal radius can be approximated by:^{3,4}

$$r_0(t) = \left(\frac{3hc K_I^d(t) z_0}{2\sqrt{2\pi} F(v(t))} \right)^{2/5} \quad (9)$$

where

$$c = \begin{cases} c_o & \text{for transmission} \\ \frac{v}{E} & \text{for reflection} \end{cases}$$

The above equations in the limit $v \rightarrow 0$ are also valid for the case of a dynamically loaded stationary crack. In a typical experiment, a high-speed camera is used to obtain a time sequence of caustics. The

diameter $D(t)$ of these caustics is measured and hence the stress intensity factor, $K_I^d(t)$, is computed using eqn (8). From eqn (9), one finds that $r_o(t) = \hat{r}_o(K_I^d(t), z_o, v(t))$ and as $K_I^d(t)$ varies with time in a dynamic experiment, the radius of the initial curve would perforce change during the course of the experiment. Thus from the point of view of experiments, it is vital to know that relation (5) based on the plane-stress approximation together with the asymptotic expression (6) lead to a valid expression for the optical path difference field for at least the range of radii that the initial curve would cover during the event of interest.

To make matters a little more explicit, suppose that during the event of interest (which could be the crack propagation phase) the initial curve radius is known from previous experience to vary in the region $r_{\min} \leq r_o \leq r_{\max}$ for some choice of the object plane distance z_o . Also, since the domain of validity of eqn (6) could in general be time-dependent as well, let a and b be such as to give the smallest annulus in which eqn (6) holds, for all times during the entire event of interest. Then, for a valid interpretation of the caustics in terms of the above formulas (eqns (8) and (9)), the inequalities $b < r_{\min} \leq r_o \leq r_{\max} < a$ must be satisfied in order to have the initial curve fall in a region of K_I^d -dominance at all times.

The first attempts to address the issue of the validity of eqns (6)–(9) are reported in Ravi-Chandar & Knauss.⁶ A series of tests were performed using the method of caustics in transmission on identical specimens under identical stress-wave loading, varying from test to test only the object plane distance z_o . In this manner a range of initial curve radii was scanned and, since presumably the actual stress-intensity factor history $K_I^d(t)$ for various tests must be identical, the apparent stress intensity factors measured from caustics obtained from different object planes must also agree, at least for those times when the initial curve falls within the region of K_I^d -dominance. Their findings indicate that the assumptions behind eqn (6) might not generally be tenable. Since a substantial part of the dynamic fracture data extant in the literature has been obtained through the use of either caustics or photoelasticity, the ramifications of the result are potentially far-reaching and thus deserve more careful scrutiny.

In particular, in the method of caustics, it would be preferable to be able to obtain the apparent stress-intensity factor values from different initial curves around the crack tip for the same specimen at any instant in time. While comparison of results across tests can be made with confidence for the loading regime of the experiments, this becomes more difficult in the crack propagation phase since small variations in

crack motion history could lead to large variations in the value of the stress intensity factor from test to test.

This problem could be circumvented if one were able to obtain caustics from different initial curves simultaneously in the same experiment. In the following section we discuss an optical configuration that would allow for the simultaneous acquisition of dynamic caustics for two different object planes (and hence two different initial curves) using a single high-speed camera.

3.2 Bifocal caustics experiments

A schematic of the optical set-up required to bring two different object planes simultaneously into focus in a single camera is shown in Fig. 4. This schematic corresponds to a reflection arrangement for caustics. The set-up entails the use of two beam-splitters and two mirrors by which two optical paths of different path lengths are established between the opaque specimen and the high-speed camera. With reference to the figure, let the high-speed camera be set up to focus at a distance f from the camera lens. Along path (1) this would mean that the virtual object plane is located at a distance z_{o1} behind the specimen. Along path (2), however, by virtue of the increased length ($2L$) between the specimen and the camera lens, the object plane would now fall only a distance $z_{o2} = z_{o1} - 2L$ behind the specimen. Thus the caustic obtained from the two paths would be from two different initial-curve radii. These two caustics could be made to appear on the film track of the high-speed camera either superposed or side by side.

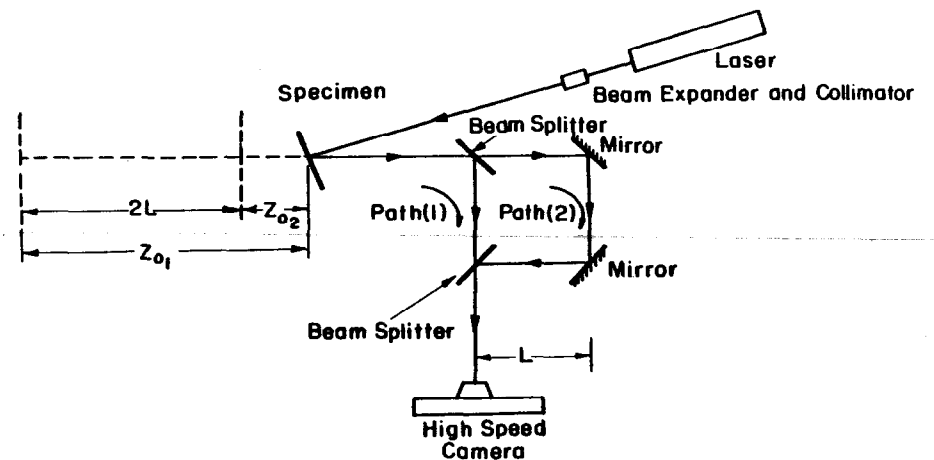


Fig. 4. Schematic diagram of reflection bifocal caustics set-up.

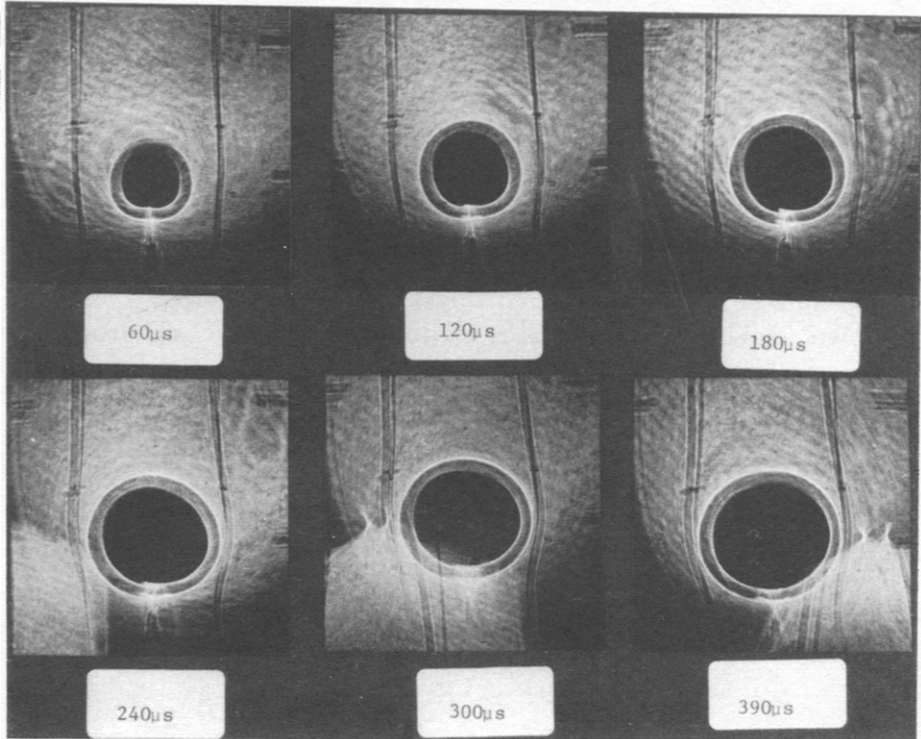


Fig. 6. Representative sequence of reflection bifocal caustics of a dynamically loaded stationary crack in AISI 4340 steel.

drop-weight tower was used as the loading device. A rotating mirror high-speed camera in conjunction with an argon-ion pulse laser was used to record a time-sequence of bifocal caustics as described earlier. The details of specimen preparation and the experimental set-up may be found in Krishnaswamy & Rosakis.¹⁵ The pairs of caustics obtained at each instant of time were analyzed as described earlier to get the apparent stress-intensity factor histories. Only representative results will be presented here. Figure 8 shows the results for the uninitiated

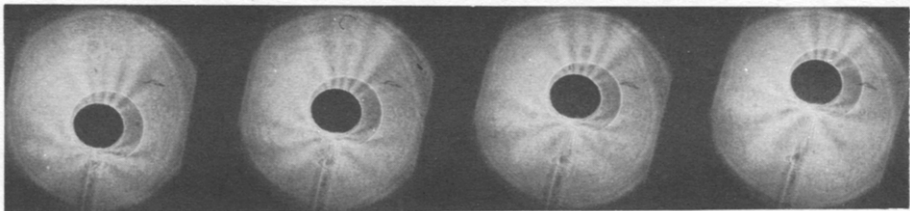


Fig. 7. Representative sequence of transmission bifocal caustics of a dynamically propagating crack in Homalite-100.

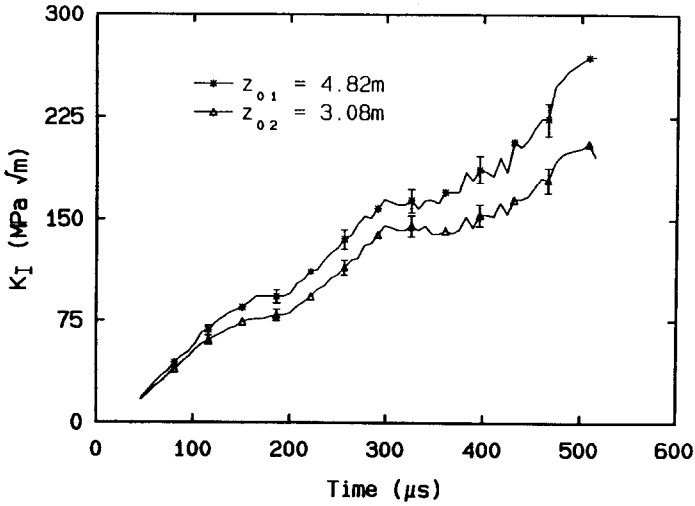


Fig. 8. K_I^d versus t plot obtained from reflection bifocal caustics of a stationary, dynamically loaded crack.

dynamically loaded crack for specimen α -3. The two apparent stress-intensity factors obtained from the diameters of the bifocal caustics pairs are shown as functions of time from impact. The object plane distances used in this experiment were $z_{01} = 4.82$ m and $z_{02} = 3.08$ m. The region of possible measurement uncertainty is indicated as vertical error bars. Figure 9 is an alternate representation of the experimental

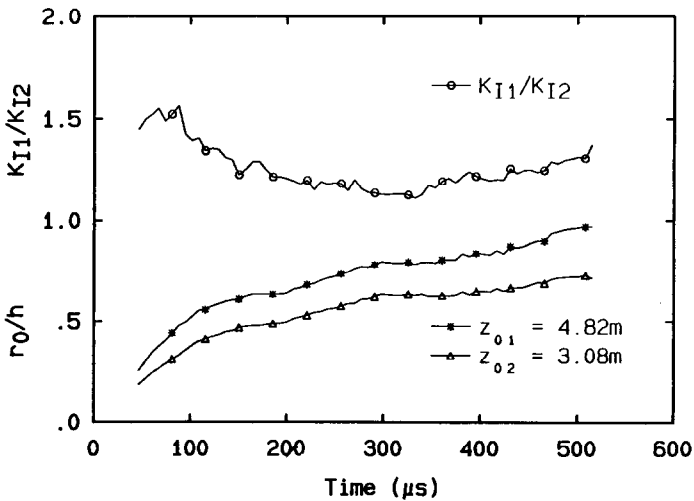


Fig. 9. Plot of K_{I1}^d/K_{I2}^d versus time from the reflection bifocal caustics experiment when a crack is stationary but dynamically loaded.

results for specimen α -3. Here the ratio of the two stress-intensity factors from the bifocal caustic pairs (K_{I1}^d/K_{I2}^d) is plotted as a function of time from impact. Also plotted as a function of time are the radii of the initial curves for the two choices of object plane distance. It is seen that the apparent measured stress-intensity factor is not quite independent of the region from which the measurement is made. Indeed, differences greater than 40% are observed between the measured stress-intensity factors obtained from initial curves whose radii vary by less than 20% of the plate thickness. Further, the larger measured stress-intensity factor corresponds to the larger object plane distance and hence the larger initial-curve radius. Unlike the results of Rosakis & Ravi-Chandar¹² for the static case, these differences persist even for $r_o/h \geq 0.5$.

A representative set of results for the crack propagation phase is shown in Fig. 10. These are again time history plots of the two measured dynamic stress-intensity factors from the bifocal caustic pairs. The larger initial curve is again seen to give a larger apparent stress-intensity factor. Differences of up to 30% in the measured values are seen in these experiments. The initial-curve radii are almost always greater than one-half the specimen thickness during the crack-propagation phase. These differences, therefore, do not disappear for $r_o/h \geq 0.5$ during the propagation phase as well (unlike the quasi-static case).

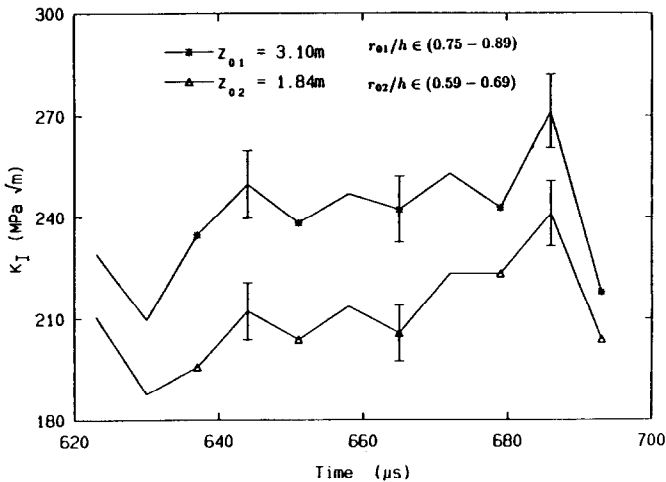


Fig. 10. Plot of K_I^d versus time from reflection bifocal caustics experiment when a crack is dynamically propagating in AISI 4340 steel.

4 TRANSIENT ASYMPTOTIC ANALYSIS OF DYNAMIC CRACK TIP FIELDS

The experimental results (obtained by means of bifocal caustic pairs), discussed in the previous section, clearly show the inadequacy of the classical analysis of caustics in accurately measuring the dynamic stress intensity factor during transient crack growth events. Even if the initial curve radius lies well outside the regions of near tip three-dimensionality, where plane stress conditions are achieved, the assumption of K_I^d -dominance (validity of relation (6) outside the three dimensional zone) clearly fails, resulting in the inconsistencies described above.

In this section, we discuss an explanation of this phenomenon by relaxing the assumption of K_I^d -dominance. While dynamic caustic patterns have conventionally been analyzed under the assumption of K_I^d -dominance, the use of higher order terms has been the recent practice in the method of photoelasticity.¹⁸ However, all available higher-order elastodynamic solutions thus far have been for the case of steadily propagating cracks, and the applicability of such solutions to highly transient problems is questionable.

We will now relax the assumption of K_I^d -dominance and examine the validity of a transient higher-order expansion for dynamic crack growth which has become available recently by Freund & Rosakis.¹⁹ Although their results hold for transient crack growth with non-uniform crack tip speed history, they also provide an expression for the special case of transient growth under constant speed. This is still a truly transient situation since field quantities are allowed to be functions of time. Here we restrict our discussion to this case since our experimental results conform with the assumption of constant speed. According to the results of Freund & Rosakis,¹⁹ the higher-order expression for $(\hat{\sigma}_{11} + \hat{\sigma}_{22})$ describing a constant velocity, transient crack tip field is given by:

$$\begin{aligned} \frac{\sigma_{11} + \sigma_{22}}{2\rho(c_1^2 - c_s^2)} &= \frac{3v^2}{4c_1^2} A_0 \cos(\theta_1/2) \cdot r_1^{-1/2} + \frac{2v^2}{c_1^2} A_1 \\ &+ \left[\left\{ \frac{15v^2}{4c_1^2} A_2 + \left(1 - \frac{v^2}{2c_1^2} \right) D^1(A_0) \right\} \cos(\theta_1/2) \right. \\ &\left. + \frac{v^2}{8c_1^2} D^1(A_0) \cos(3\theta_1/2) \right] \cdot r_1^{1/2} \end{aligned}$$

$$\begin{aligned}
& + \left[\left\{ \frac{6v^2}{c_1^2} A_3 + \left(1 - \frac{v^2}{4c_1^2} \right) D^1(A_1) \right\} \cos(\theta_1) \right] \cdot r_1 \\
& + \left[\left\{ \frac{35v^2}{4c_1^2} A_4 + \left(1 - \frac{v^2}{2c_1^2} \right) D^1(A_2) \right. \right. \\
& \left. \left. + \frac{1}{9} \left(1 - \frac{v^2}{4c_1^2} \right) D^2(A_0) + \left(1 - \frac{v^2}{2c_1^2} \right) \ddot{A}_0 \right\} \cos(3\theta_1/2) \right. \\
& \left. + \left\{ \frac{3v^2}{8c_1^2} D^1(A_2) + \frac{1}{6} \left(1 - \frac{v^2}{4c_1^2} \right) D^2(A_0) + \frac{3}{8} \ddot{A}_0 \right\} \cos(\theta_1/2) \right. \\
& \left. + \left\{ \frac{v^2}{96c_1^2} D^2(A_0) \right\} \cos(5\theta_1/2) \right] \cdot r_1^{3/2} \\
& + \left[\left\{ \frac{12v^2}{c_1^2} A_5 + \left(1 - \frac{v^2}{2c_1^2} \right) D^1(A_3) + \frac{D^2(A_1)}{16} + \left(1 - \frac{v^2}{2c_1^2} \right) \ddot{A}_1 \right\} \cos(2\theta_1) \right. \\
& \left. + \left\{ \frac{v^2}{2c_1^2} D^1(A_3) + \frac{1}{8} \left(1 - \frac{v^2}{4c_1^2} \right) D^2(A_1) + \frac{1}{2} \ddot{A}_1 \right\} \right] \cdot r_1^2 + o(r_1^2) \quad (10)
\end{aligned}$$

where the differential operators $D^1(\cdot)$ and $(\ddot{\cdot})$ are defined as follows:

$$D^1(A_k) \equiv \frac{v}{(c_1^2 - v^2)} \frac{d}{dt} \{A_k\} (k+3) \quad k = 0, 1, 2, \dots$$

$$D^2(A_k) \equiv D^1(D^1(A_k))$$

and

$$\ddot{A}_k = \left(\frac{d^2}{dt^2} A_k \right) / (c_1^2 - v^2) \quad A_k = A_k(t)$$

Note that the spatial variation of the terms associated with coefficients A_k are identical to the ones that should be obtained from a higher-order steady state analysis. Of course, in the general transient case, A_k are functions of time and crack tip velocity. Also, $D^1(A_k)$, $D^2(A_k)$ and \ddot{A}_k depend on time derivatives of the time dependent coefficients A_k . For example

$$D^1(A_0) = -\frac{3v^{1/2}}{(c_1^2 - v^2)} \frac{d}{dt} \{A_0 v^{1/2}\}$$

where

$$A_0(t) = \frac{4 K_1^d(t)}{3 \mu \sqrt{2\pi}} \frac{(1 + \alpha_s^2)}{[4\alpha_s \alpha_1 - (1 + \alpha_s^2)^2]}, \quad \alpha_{1,s}^2 = \left(1 - \frac{v^2(t)}{c_{1,s}^2} \right)$$

Thus, $D^1(A_0)$ is related to the first time derivatives of the stress intensity factor and velocity history.

By using the transient field given in eqn (10) and re-arranging terms, one can obtain a relation involving the x_1 gradient of $(\hat{\sigma}_{11} + \hat{\sigma}_{22})$ as follows:

$$\begin{aligned}
 Y_I^d(r_1, \theta_1) &= \frac{\partial(\hat{\sigma}_{11} + \hat{\sigma}_{22})}{\partial x_1} \frac{2\sqrt{2\pi} r_1^{3/2}}{F(v) \cos \frac{3\theta_1}{2}} \\
 &= K_I^d + \left\{ \beta_1 \frac{\cos \frac{\theta_1}{2}}{\cos \frac{3\theta_1}{2}} + \beta_2 \frac{\cos \frac{5\theta_1}{2}}{\cos \frac{3\theta_1}{2}} \right\} r_1 \\
 &\quad + \beta_3 r_1^{3/2} \frac{1}{\cos \frac{3\theta_1}{2}} + r_1^2 \left\{ \beta_4 \frac{\cos \frac{\theta_1}{2}}{\cos \frac{3\theta_1}{2}} + \beta_5 + \beta_6 \frac{\cos \frac{7\theta_1}{2}}{\cos \frac{3\theta_1}{2}} \right\} \\
 &\quad + \beta_7 r_1^{5/2} \frac{\cos \theta_1}{\cos \frac{3\theta_1}{2}} + o(r_1^{5/2}) \tag{11}
 \end{aligned}$$

where

$$F(v) = \frac{2(1 + \alpha_s^2)(\alpha_1^2 - \alpha_s^2)}{[4\alpha_1\alpha_s - (1 + \alpha_s^2)^2]}$$

and $\beta_1, \beta_2, \beta_3, \dots, \beta_7$ are functions of time related to the coefficients of relation (10).

At each time instant under K_I^d -dominance, $Y_I^d(r_1, \theta_1)$ is a constant and equal to the instantaneous stress intensity factor K_I^d . If significant higher-order transient terms exist, then the spatial variation of $Y_I^d(r_1, \theta_1)$ will be given by the right hand side of eqn (11).

4.1 CGS experiments

A new full field optical technique, Coherent Gradient Sensing (CGS) has recently been developed by Tippur *et al.*⁸ for measuring crack tip deformation fields. The method can be used either in a transmission or a reflection mode and like caustics is sensitive to deformation induced gradients in the optical path. In transmission these gradients are due to refractive index changes while in reflection these are due to non-uniform surface slopes. This technique, which is described in detail in Ref. 8, has similarity to the method of caustics regarding the deformation quantities it measures, and it can be used as easily to study crack

growth in both transparent and opaque solids. Using this technique, validity of relations (10) and (11) has recently been studied by Krishnaswamy *et al.*²⁰ In this work, the method of Coherent Gradient Sensing has been used to demonstrate the accuracy of the higher-order transient expansion in describing the crack tip stress fields during the unsteady dynamic crack growth.

Figure 11 shows a selection of CGS interferograms corresponding to dynamic crack growth in impact loaded, three-point bend specimens made of PMMA. A rotating mirror high-speed camera and a pulsed laser light source is used to record the CGS patterns. Here we have a transmission optical arrangement and the fringes correspond to contours of equal $(\partial/\partial x_1)(\hat{\sigma}_{11} + \hat{\sigma}_{22})$. The details of the experimental set-up are given by Krishnaswamy *et al.*²⁰

Figure 12 shows the analysis of an interferogram corresponding to time $t = 20 \mu\text{s}$ after crack initiation. The crack tip velocity is approximately 300 m/s. In this early time it is expected that transient effects are still important. The figure shows the variation of Y_1^d versus normalized radial distance (r_1/h) for different radial lines ($\theta_1 = 0, 30^\circ, 45^\circ, 120^\circ$)

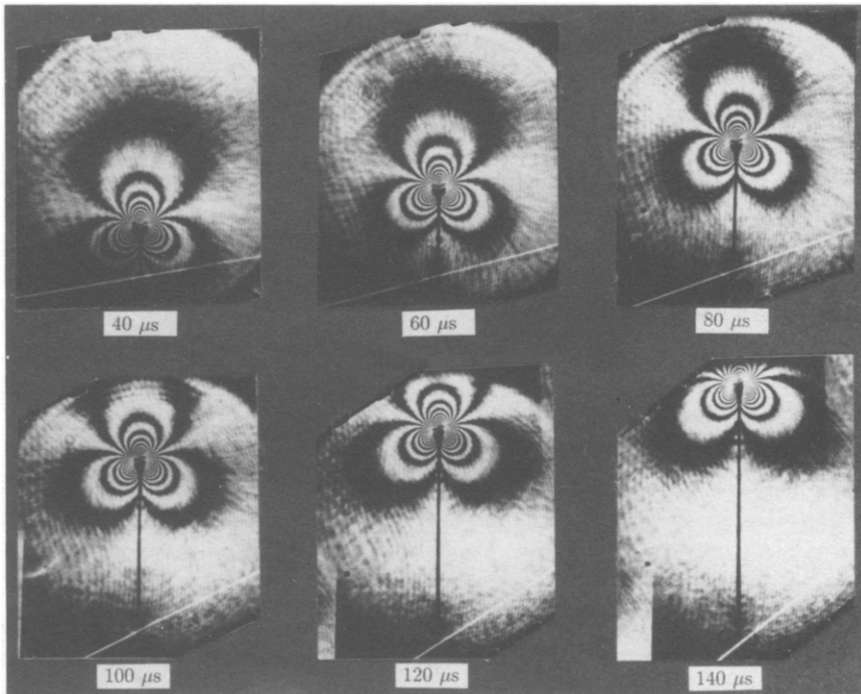


Fig. 11. CGS interference patterns around a dynamically propagating crack in PMMA ($v \sim 300 \text{ m/s}$).

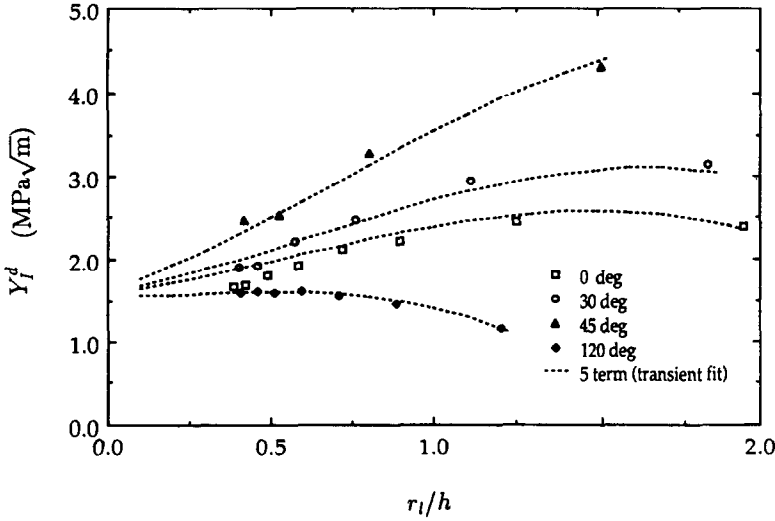


Fig. 12. Plot of Y_I^d versus (r_l/h) along different radial directions around a propagating crack ($20 \mu s$ after crack initiation) in PMMA.

around the propagating crack tip. As is apparent from the figure, there appears to be no region around the crack tip over which Y_I^d is constant. Indeed, the spread in Y_I^d values from different locations is as much as 400%. Thus, extraction of dynamic stress intensity values obviously cannot be based here on a simplistic assumption of near tip K_I^d -dominance. The figure also contains the results of a least-squares procedure of the fitting of relation (11) to the experimental data Y_I^d obtained from the CGS interferogram. The fitted expression (dotted line) corresponds to the six-term transient expansion for $\hat{\sigma}_{11} + \hat{\sigma}_{22}$ (five terms for $(\partial/\partial x_1)(\sigma_{11} + \sigma_{22})$) and seems to capture all the essential features of the experimental results for all values of r_l and θ_l that lie outside the near-tip 3-D zone whose maximum extent is $r_l/h = 0.5$.

In the reflection mode, CGS fringe patterns correspond to contours of equal $\partial u_3/\partial x_1$. Recalling that for plane stress deformations

$$\frac{\partial u_3}{\partial x_1} = \frac{-\nu}{E} \frac{\partial}{\partial x_1} (\hat{\sigma}_{11} + \hat{\sigma}_{22})$$

relation (11) will be modified to give:

$$Z_I^d(r_l, \theta_l) = \left(\frac{\partial u_3}{\partial x_1} \right) \frac{1}{F(\nu)} \frac{4\sqrt{2\pi} E}{\nu h} \frac{r_l^{3/2}}{\cos \frac{3\theta_l}{2}}$$

$$\begin{aligned}
&= K_1^d + \left\{ \delta_1 \frac{\cos \frac{\theta_1}{2}}{\cos \frac{3\theta_1}{2}} + \delta_2 \frac{\cos \frac{5\theta_1}{2}}{\cos \frac{3\theta_1}{2}} \right\} r_1 \\
&\quad + \delta_3 r_1^{3/2} \frac{1}{\cos \frac{3\theta_1}{2}} + r_1^2 \left\{ \delta_4 \frac{\cos \frac{\theta_1}{2}}{\cos \frac{3\theta_1}{2}} + \delta_5 + \delta_6 \frac{\cos \frac{7\theta_1}{2}}{\cos \frac{3\theta_1}{2}} \right\} \\
&\quad + \delta_7 r_1^{5/2} \frac{\cos \theta_1}{\cos \frac{3\theta_1}{2}} + o(r_1^{5/2})
\end{aligned}$$

where $\delta_1, \delta_2, \dots, \delta_7$ are functions of time.

Lack of K_1^d -dominance here implies that $Z_1^d(r_1, \theta_1)$ is not constant. To demonstrate this in a reflection arrangement, a series of dynamic fracture tests were performed again using impact loaded three-point bend specimens made of PMMA. The front planar surface of the specimen was coated with a reflective aluminum coating by means of vacuum deposition. The reflection CGS arrangement described by Krishnaswamy *et al.*²⁰ was used to obtain fringe patterns of the type shown in Fig. 13. Typically a six term expansion in $\delta_{11} + \delta_{22}$ was found

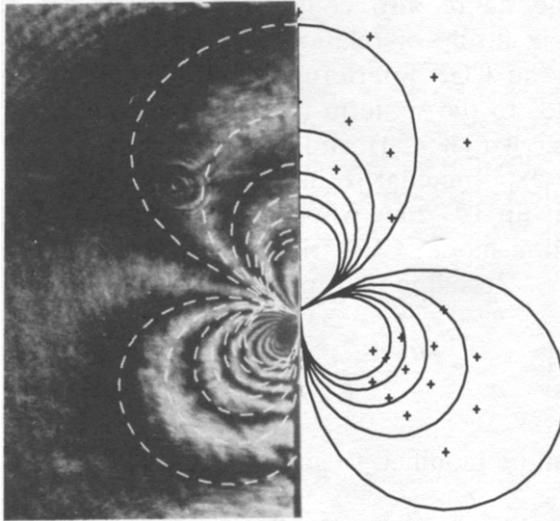


Fig. 13. Left: Superposition of a six-term transient expansion fit and the corresponding reflection CGS pattern of a dynamically propagating crack in PMMA. Right: Data points (crosses) used in the least square analysis and the corresponding K_1^d -dominant fit.

to be necessary to adequately describe the crack tip fields. To provide a visual demonstration of the agreement between the six term fit and the experimental data, a reconstructed fringe pattern from the transient fit is shown superimposed on the interferogram in Fig. 13. Here the broken lines represent the fringe pattern reconstructed from the transient high-order fit. Also shown in the right half of the picture is a fringe pattern reconstructed from only the term associated with K_I^d (term of order $r_1^{-1/2}$ in the stresses). It is obvious from this comparison that the one term field description fails to describe the experimental fringe pattern.

Finally Fig. 14 shows the variation of Z_I^d with normalized radial distance (r_1/h) for different radial lines ($\theta_1 = 0, 15^\circ, 30^\circ, 120^\circ$). Again, and as in the transmission case, Z_I^d is clearly not a constant as would be expected for K_I^d -dominance. On the other hand, the experimental measurement (discrete points) falls very close to the analytical result of the transient high order expansion, at least for $r_1/h > 0.5$ (extent of the 3-D zone).

As evident from the above results for the cases discussed, the assumption of asymptotic K_I^d -dominance fails in the plane stress region surrounding the near tip three-dimensional zone. It is therefore expected that caustic patterns obtained from such regions and

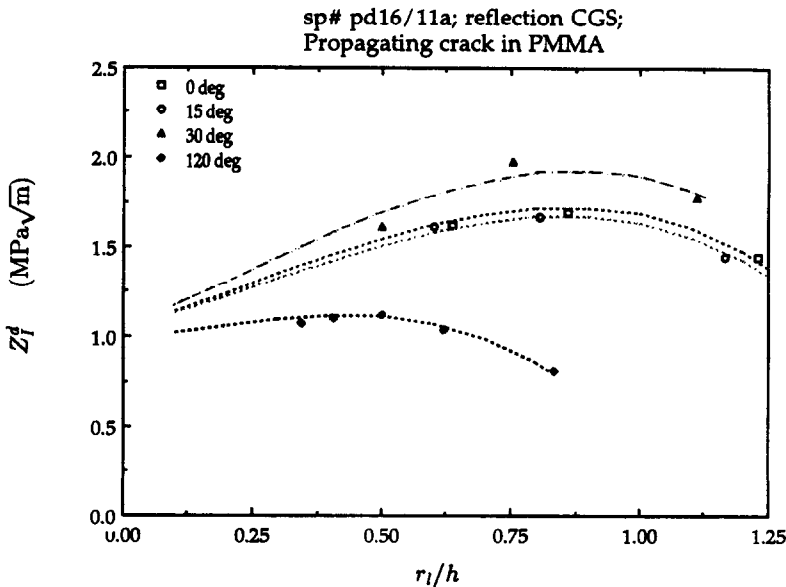


Fig. 14. Z_I^d versus (r_1/h) along different radial directions around a propagating crack in PMMA.

analyzed by using the classical analysis of caustics (see Section 3, eqns (6)–(9)) would not yield the correct value of stress intensity factor. This is true because such cases the crack tip fields are not well approximated by the single term expression (6).

4.2 Synthetic caustics

In order to demonstrate the above conjuncture conclusively and to illustrate the inadequacy of the classical analysis of caustics for analyzing truly transient crack growth phenomena, the following procedure is adopted.

From the multi-parameter analysis of the $(\partial(\hat{\sigma}_{11} + \hat{\sigma}_{22})/\partial x_1)$ patterns obtained using CGS transmission (described in the previous section), one can obtain $K_I^d, \beta_1, \beta_2, \beta_3, \dots$. Once these constants are determined, $(\partial/\partial x_2)(\hat{\sigma}_{11} + \hat{\sigma}_{22})$ can be calculated using the expression for $(\hat{\sigma}_{11} + \hat{\sigma}_{22})$. Now, let us remember that the caustic mapping in transmission is given by:

$$X_\alpha = x_\alpha + z_0 \left[c_\sigma h \frac{\partial}{\partial x_\alpha} (\hat{\sigma}_{11} + \hat{\sigma}_{22}) \right], \quad \alpha = 1, 2$$

where (X_1, X_2) denote the in-plane coordinates of the caustic plane located at a distance z_0 from the specimen plane (x_1, x_2) along the optical axis. Using the above mapping, caustics have been generated from the CGS fringe patterns. One such caustic for a time instant $20 \mu\text{s}$

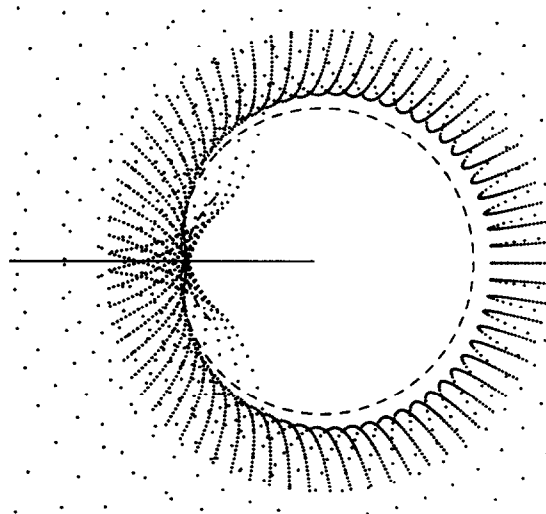


Fig. 15. Synthetic caustic obtained by analyzing transmission CGS pattern for a time instant $20 \mu\text{s}$ after crack initiation.

after crack initiation is shown in Fig. 15. The image plane distance ($z_0 = 6\text{ m}$) is such that the initial curve radius is well outside the crack tip 3-D region ($r_0 \sim 1.04h$). If one were to synthetically plot the caustic based only on the value of K_I^d (determined from a multi-parameter transient fit to the CGS pattern), the caustic should look like the one shown by the broken line.

This clearly demonstrates the effect of transient higher-order terms on the diameter of the caustic. The effect in the computed value of K_I^d is expected to be even more pronounced. Indeed, if the synthetic caustic is now interpreted in the classical way, as if it were generated by a K_I^d -field (see eqn (8)), the resulting value is found to be 25–30% higher than the value of K_I^d obtained from the full field measurements which were input in the numerical calculation. To demonstrate this clearly, the value of $K_I^d(t)$ measured from the full field CGS patterns, using the transient higher-order fit, for different times after crack initiation are plotted in Fig. 16. Also in the same plot, values of K_I^d -caustic obtained by interpreting the synthetic caustic (generated from the experimental field measurements) in the classical manner are displayed. The figure clearly shows a persistent difference of the order discussed above which is due to the violation of the assumption of strict K_I^d -dominance during transient crack growth.

Indeed this is consistent with the results of the bifocal caustics experiments presented in Section 3, where pairs of caustics simultaneously generated from different distances from the crack tip, during

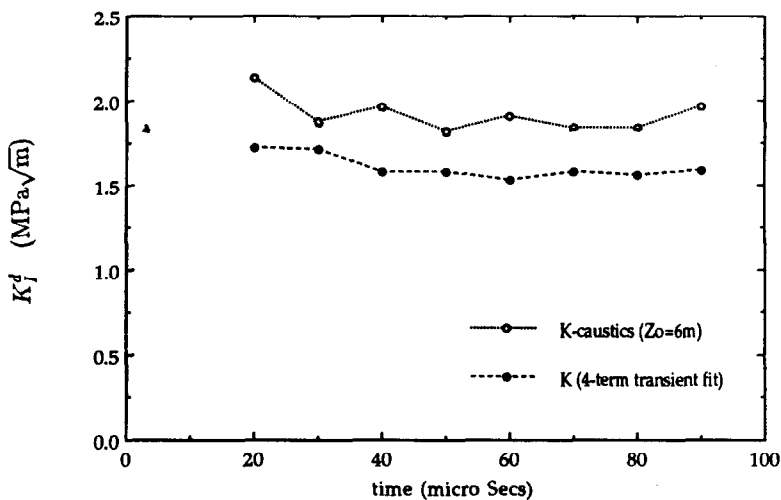


Fig. 16. Plot of K_I^d -caustic and K_I^d -CGS at different times during crack growth in PMMA. (Range of r_0/h for K_I^d -caustic: 0.98–1.04.)

crack growth, and analyzed in the conventional way also resulted in differences in K_I^d of the same order.

5 CONCLUSIONS

In this work we discuss several possible sources of inaccuracy that may arise in the classical interpretation of caustic patterns obtained during dynamic crack growth in nominally elastic materials. A modified caustics set-up (bifocal caustics arrangement) and a new full field optical technique called 'Coherent Gradient Sensing' are used in this investigation. Based on the results obtained from these two independent techniques, we emphasize the following points:

1. The existence of a near-tip three-dimensional zone excludes the possibility of interpreting caustic patterns that are obtained from distances smaller than one half of the specimen thickness from the crack tip.
2. For distances from the crack tip greater than half the specimen thickness, where plane stress conditions exist, the classical interpretation of caustic patterns is possible only if the surrounding field is strictly K_I^d -dominant (well approximated by the $r^{-1/2}$ singular term of the plane stress asymptotic expansion).
3. In most transient crack growth events K_I^d -dominance is not generally observed, especially at times close to crack initiation or arrest. This is also true in laboratory size specimens where stress wave reflections may produce non-uniform stress-intensity factor histories. In such cases a truly transient higher order expansion is necessary for correctly describing stress fields outside the crack-tip three-dimensional zone.
4. Under transient crack growth conditions, use of the classical analysis of caustics in the interpretation of the optical patterns may result in errors that could exceed 30% in the value of the stress intensity factor.

ACKNOWLEDGEMENTS

Support of ONR through Contract N00014-90-J-1340 and of NSF through the Presidential Young Investigator Award (Grant MSM-84-512040) to AJR is gratefully acknowledged. The authors would like to

acknowledge the contribution of Mr R. Pfaff toward upgrading the high-speed camera of GALCIT. The authors are also thankful to Professor L. B. Freund of Brown University for many helpful discussions and suggestions during the course of this investigation.

REFERENCES

1. Manogg, P., Anwendungen der Schattenoptik zur Untersuchung des Zerreißvorgangs von Platten. Doctoral Dissertation, Freiburg, West Germany, 1964.
2. Theocaris, P. S., Elastic stress intensity factors evaluated by caustics. In *Mechanics of Fracture*, Vol. VII ed. G. C. Sih, Sijthoff and Noordhoff, Rockville, USA, 1981.
3. Beinert, J. & Kalthoff, J. F., Experimental determination of dynamic stress intensity factors by shadow patterns. *Mechanics of Fracture*, Vol VII ed. G. C. Sih, Sijthoff and Noordhoff, Rockville, USA, 1981.
4. Rosakis, A. J., Duffy, J. & Freund, L. B., The determination of the dynamic fracture toughness of AISI 4340 steel by the shadow spot method. *Journal of the Mechanics and Physics of Solids*, **34**(4) (1984) 443–60.
5. Zehnder, A. T. & Rosakis, A. J., Dynamic fracture initiation and propagation in 4340 steel under impact loading. Caltech Report SM 86-6 (to appear in the *International Journal of Fracture*) (1986).
6. Ravi-Chandar, K. & Knauss, W. G., On the characterization of the transient stress fields near the tip of a crack. *Journal of Applied Mechanics*, **54** (1987) 72–8.
7. Rosakis, A. J. & Zehnder, A. T., On the method of caustics: an exact analysis based on geometrical optics. *Journal of Elasticity*, **4** (1985) 347–67.
8. Tippur, H. V., Krishnaswamy, S. & Rosakis, A. J., Optical mapping of crack tip deformation using the methods of transmission and reflection coherent gradient sensing. *Caltech Report SM 89-11* (submitted to the *International Journal of Fracture*) (1989).
9. Zehnder, A. T. & Rosakis, A. J., Three dimensional effects near a crack tip in a ductile three point bend specimen, Part II: An experimental investigation using interferometry and caustics. Caltech Report SM 88-7 (to appear in the *Journal of Applied Mechanics*) (1988).
10. Rosakis, A. J., Zehnder, A. T. & Narasimhan, R., Caustics by reflection and their application to dynamic and elastic-plastic fracture mechanics. *Optical Engineering*, **27** (8) (1988) 596–610.
11. Zehnder, A. T., Rosakis, A. J. & Krishnaswamy, S., Dynamic Measurement of the J -integral in ductile metals: comparison of experimental and numerical techniques. *Proceedings of IUTAM Symposium on Recent Advances in Non-Linear Fracture Mechanics*, Caltech, 1988; (also, Caltech Report SM 88-8, to appear in the *International Journal of Fracture*).
12. Rosakis, A. J. & Ravi-Chandar, K., On the crack tip stress state: an experimental evaluation of three dimensional effects. *International Journal of Solids and Structures*, **22** (2) (1986) 121–34.

13. Narasimhan, R. & Rosakis, A. J., Three dimensional effects near a crack tip in a ductile three point bend specimen, Part I: Numerical investigations. Caltech Report SM 88-6 (to appear in the *Journal of Applied Mechanics*) (1988).
14. Yang, W. & Freund, L. B., *International Journal of Solids and Structures*, **21**(9) (1985) 977-94.
15. Krishnaswamy, S. & Rosakis, A. J., On the extent of dominance of asymptotic elastodynamic crack tip fields, Part I: An experimental study using bifocal caustics. Caltech Report SM 88-21 (submitted to the *Journal of Applied Mechanics*).
16. Freund, L. B. & Clifton, R. J., On the uniqueness of plane elasto-dynamic solutions for running cracks. *Journal of Elasticity*, **4**(4) (1974) 293-9.
17. Rosakis, A. J., Analysis of the optical method of caustics for dynamic crack propagation. *Engineering Fracture Mechanics*, **13** (1980) 331-47.
18. Dally, J. W., Fourny, W. L. & Irwin, G. R., On the uniqueness of $K_{ID}-\dot{a}$ relation. *International Journal of Fracture*, **27** (1985) 159-68.
19. Freund, L. B. & Rosakis, A. J., The influence of transient effects on the asymptotic crack tip field during dynamic crack growth. 11th National Congress of Applied Mechanics, Tucson, Arizona, May 1990.
20. Krishnaswamy, S., Tippur, H. V. & Rosakis, A. J., Measurement of transient crack tip deformation fields using the method of coherent gradient sensing. Caltech Report SM 90-1 (submitted to the *Journal of the Mechanics and Physics of Solids*) (1990).